A multiscale 3D chemotaxis assay reveals bacterial navigation mechanisms

Marianne Grognot
Rowland Institute at Harvard https://orcid.org/0000-0002-7491-1224
Katja Taute (taute@rowland.harvard.edu)
Harvard University https://orcid.org/0000-0003-2230-717X

Article

Keywords: Bacteria Motility, 3D Trajectories, Surface Effects

Posted Date: September 11th, 2020

DOI: https://doi.org/10.21203/rs.3.rs-61942/v1

Version of Record: A version of this preprint was published at Communications Biology on June 3rd, 2021. See the published version at https://doi.org/10.1038/s42003-021-02190-2.

A multiscale 3D chemotaxis assay reveals bacterial navigation mechanisms

Marianne Grognot & Katja M. Taute*
Rowland Institute at Harvard University, 100 Edwin H. Land Blvd, Cambridge, MA 02142, US
*corresponding author: taute@rowland.harvard.edu

Abstract

How motile bacteria navigate environmental chemical gradients has implications ranging from health to climate science, but the underlying behavioral mechanisms are unknown for most species. The well-studied navigation strategy of *Escherichia coli* forms a powerful paradigm that is widely assumed to translate to other bacterial species. This assumption is rarely tested because of a lack of techniques capable of bridging scales from individual navigation behavior to the resulting population-level chemotactic performance.
Here, we present such a multiscale 3D chemotaxis assay by combining high-throughput 3D bacterial tracking with microfluidically created chemical gradients. Large datasets of 3D trajectories yield the statistical power required to assess chemotactic performance at the population level, while simultaneously resolving the underlying 3D navigation behavior for every individual. We demonstrate that surface effects confound typical 2D chemotaxis assays, and reveal that, contrary to previous reports, *Caulobacter crescentus* breaks with the *E. coli* paradigm.

Introduction

Chemotaxis enables bacteria to navigate external chemical fields and is now recognized as a key factor driving interactions of bacteria with their environment and each other, with wide-ranging effects that include promoting pathogenicity[1], establishing symbioses[2], and shaping geochemical fluxes[3]. Because individual bacterial motility behavior has a large random component, chemotaxis is usually assessed using population-level assays that average over the behavior of thousands of individuals, ranging from Adler's classic capillary assay[4] to modern approaches based on video microscopy[5]. While these approaches are highly sensitive and precise in detecting small chemotactic effects, they are blind to the underlying behavioral mechanisms. Berg's pioneering 3D tracker capable of following a single bacterium swimming in 3D demonstrated the importance of resolving individual 3D motility behavior for revealing chemotactic mechanisms[6]. The resulting understanding that *Escherichia coli* chemotaxis is controlled via the bias in the rotation direction of the flagellum[7] has become a dominant paradigm in bacterial chemotaxis research[8]. Recent findings, however, suggest that many other species, including the majority of marine bacteria, may use a different strategy[9,10], highlighting the need for efficient and broadly applicable methods of characterizing chemotactic behavior.

The pervasive inter-individual variability present even in genetically identical populations[11] renders throughput and sampling crucial bottlenecks in characterizing chemotactic behavior based on trajectory data. Methods aimed at revealing potentially diverse chemotactic

mechanisms must bridge the scales between individuals and populations by capturing motility behavior of individual bacteria with the statistical power to simultaneously reveal chemotactic performance, which is typically only accessible via ensemble averages. Here we introduce a novel chemotaxis assay that enables such a multiscale approach by harnessing a recently developed high-throughput 3D tracking method[12] to capture individual navigation behavior in the presence of microfluidically created chemical gradients for thousands of bacteria within minutes. After validating our approach using the well-characterized *E. coli* model system, we demonstrate its power by revealing that the chemotactic mechanism of the freshwater bacterium *Caulobacter crescentus* breaks with the *E. coli* paradigm.

Results and Discussion

Multiscale assay accurately quantifies *E. coli* chemotaxis

In our assay, typically 50-100 bacteria are tracked simultaneously in 3D in the center of a quasi-static, linear gradient field created in a microfluidic device (Fig. 1a, Supplementary Fig. 1a-d, Methods). Typically, thousands of trajectories are gathered in minutes, enabling a precise determination of the chemotactic drift velocity, v_d, as the population-averaged velocity along the direction of the gradient (x) (Fig. 1b). We demonstrate the technique by assessing chemotaxis of the well characterized *E. coli* strain AW405 towards the non-metabolizable chemoattractant α-methyl-DL-aspartate (MeAsp, Fig. 1b-e, Supplementary Fig. 2e). The population-averaged drift velocity of 2.7 ± 0.3 μm/s (mean ± SD) for bulk trajectories in a linear gradient of 10 μM/mm MeAsp aligns well with values imputed from previous work (Supplementary Discussion), confirming that our technique provides an accurate quantification of chemotactic performance.

E. coli's chemotactic drift decreases near the chamber surface

Resolving the drift velocity, v_d, as a function of vertical position, z, reveals that the drift velocity is roughly constant in the bulk liquid, but decreases sharply near the surfaces of the sample chamber (Fig. 1d, Supplementary Fig. 2f). We attribute this decrease to trajectory curvature at the surfaces (Fig. 1c) randomizing bacterial orientations and thus leading to a decreased chemotactic response. Such curvature results from hydrodynamic interactions with the surface[13] and is thus present in common 2D motility assays that increase trajectory durations by either constraining the bacteria to a thin sample chamber[14] or by limiting observations to a chamber surface[15]. In addition, our findings indicate that many standard 2D chemotaxis assays may be confounded by surface effects in their ability to quantify chemotactic performance, demonstrating the value of 3D tracking.

Multiscale assay captures *C. crescentus* chemotaxis and reveals phenotypically distinct swarmer cell populations

To demonstrate the power of our approach for revealing novel chemotactic behaviors, we turn to the fresh water bacterium *C. crescentus* whose weak, cell cycle-dependent chemotaxis response[16,17] has been challenging to capture. In *C. crescentus*'s life cycle, cell division occurs in stalked sessile cells and produces swarmer cells whose "run-reverse-flick" motility[9,18] is driven by a single polar flagellum. Either direction of flagellar rotation results in locomotion, with the

flagellum either pushing the cell body forward or pulling it backward. Reversals (turns by ~180°) occur with the transition from pushing to pulling, whereas the opposite transition is accompanied by a so-called flick, an approximately right-angle turn (Fig. 2a).

We recorded 79,244 individual 3D bulk trajectories of motile *C. crescentus* cells navigating a 1 mM/mm xylose gradient (Methods, Supplementary Table 2). Strikingly, 54% of the more than 123,000 s of total trajectory time we obtained consists of straight trajectories with no turns and no discernible chemotactic drift up the gradient. A statistical analysis of individual turn event frequencies supports the notion that these "smooth swimmers" form a phenotypically distinct group (Supplementary Discussion). In *C. crescentus*'s life cycle, the swarmer-to-sessile cell transition is accompanied by intracellular biochemical changes that may favor smooth swimming, including the degradation of chemoreceptors[17] and a rise in c-di-GMP[19] (Supplementary Discussion). While we do not know the origin of the smooth-swimming population, one possibility is that it represents the early stages of the swarmer-to-sessile cell transition. Smooth swimming is likely to accelerate the rate of surface encounters and may be an integral part of *C. crescentus*'s strategy for completing the swarmer-to-sessile cell transition[19].

The chemotactic drift speed of the remaining, turning population amounts to only 0.26 ± 0.12 µm/s (mean ± SEM), corresponding to less than 0.5% of their average swimming speed of 56 µm/s. To our knowledge, this is the first measurement of a chemotactic drift speed in *C. crescentus*, demonstrating the sensitivity enabled by the high throughput of our technique. The speed of backward runs, with the flagellum pulling the cell, is 2.5 ± 0.2% higher than that of forward ones (Supplementary Fig. 2e). Forward and backward run duration distributions are approximated well by inverse Gaussian distributions (Supplementary Fig. 2f), consistent with previous reports[15,20].

C. crescentus performs chemotaxis at near-constant bias

C. crescentus chemotaxis has been assumed to follow the *E. coli* paradigm, where the cytoplasmic concentration of phosphorylated CheY ([CheY-P]), the chemotaxis response regulator, modulates the fraction of the time that the flagella rotate clockwise, the so-called clockwise bias[19,20]. In *E. coli*, counterclockwise (CCW) rotation supports locomotion ("runs"), whereas clockwise (CW) rotation induces reorientation events ("tumbles") (Fig. 2b). Chemotaxis is achieved by dynamic modification of the bias so as to increase the duration of runs aligned with the gradient direction. Early studies hypothesized that in *C. crescentus,* forward runs driven by CW rotation correspond to *E. coli* runs, while backward runs driven by CCW rotation are equivalent to *E. coli* tumbles because of their shorter duration[21,22]. Given similar forward and backward swimming speeds, a bias towards CW rotation would then yield net displacements in the forward swimming direction. In line with this hypothesis, a recent study of 2D surface swimming behavior in oxygen gradients found that forward, but not backward runs, are extended when directed up the gradient compared to down[15].

In contrast with this hypothesis, we find that both forward and backward run segments are extended when ascending, versus descending, a chemoattractant gradient (Fig. 2c, Supplementary Fig. 2f). In fact, our data support a constant motor bias, that is, a constant ratio of forward vs backward swimming interval durations (Fig. 2f) and thus indicate a radical break with the *E. coli* paradigm of motor bias-driven chemotaxis in *C. crescentus*. We propose that, in *C. crescentus*, [CheY-P] lowers the energy barrier between the two rotation states, but leaves the

states' relative energy levels unchanged, thus modulating switching rates without affecting the motor bias[10] (Fig. 2d, Supplementary Discussion). This interpretation is also consistent with the puzzling previous observation that, in sharp contrast to *E. coli*[11], *C. crescentus* shows hardly any variability in motor bias between individuals[20], suggesting that its motor bias might be unaffected by cytoplasmic fluctuations in [CheY-P].

3D tracking overcomes limitations of 2D chemotaxis assays

The apparent conflict with previous findings[15] likely results from a technical artefact imposed by the constraints of 2D tracking: to increase the typical time a bacterium spends in the focal plane, 2D bacterial tracking had been performed at the sample chamber surface which hydrodynamically attracts the bacteria[23]. The surface-induced trajectory curvature is more pronounced in the backward than in the forward runs[15,24] (Supplementary Fig. 2g), thus likely diminishing the chemotactic response more strongly for backward than for forward runs. Placing the focal plane in the bulk can prevent such surface effects in 2D tracking but incurs severely shortened trajectories that are less likely to fully capture runs whose orientation can be assigned based on their bordering turning events. We estimate that, under typical 2D tracking conditions, approximately 30 - 40 times as much data would need to be obtained to detect the dependence of run duration on orientation relative to the gradient at similar fidelity (Supplementary Discussion, Supplementary Figure 3). This example, together with the finding of a decreased drift velocity for *E. coli* close to surfaces, highlights the crucial significance of full 3D behavioral information when assessing chemotactic mechanisms: 3D tracking enables the acquisition of long trajectories without a need for bacterial confinement as well as accurate turning angle measurements for determining bacterial orientation even for short trajectories with few turning events.

Beyond the *E. coli* paradigm

The mechanism we unveil for the alpha proteobacterium *C. crescentus* aligns with recent findings for the singly flagellated gamma proteobacteria *Vibrio alginolyticus*[9] and *Pseudomonas aeruginosa*[10]. These species also extend both forward and backward swimming intervals during chemotaxis, suggesting that this mechanism may be much more common than previously assumed. To our knowledge, no species with polar flagella has conclusively been shown to follow the *E. coli* scheme, raising the intriguing possibility that the influential *E. coli* paradigm may reflect a special case limited to species that share its flagellation pattern. We note that, despite the stark contrast in motor switching schemes, the resulting swimming pattern suggests a unified behavioral paradigm: any run in a favorable direction is extended.

In summary, our multiscale technique offers unprecedented, simultaneous access to individual and population-level 3D motility behavior and is poised to offer unique insights into novel chemotactic mechanisms as well as into the effects of phenotypic heterogeneity on population-level motility behaviors. In contrast to many flow-based chemotaxis assays[25] that are limited to liquid environments, our assay is compatible with environments such as hydrogels that more closely mimic the complexities of many natural habitats, and thus paves the way for studies of chemotactic mechanisms in ecologically relevant settings.

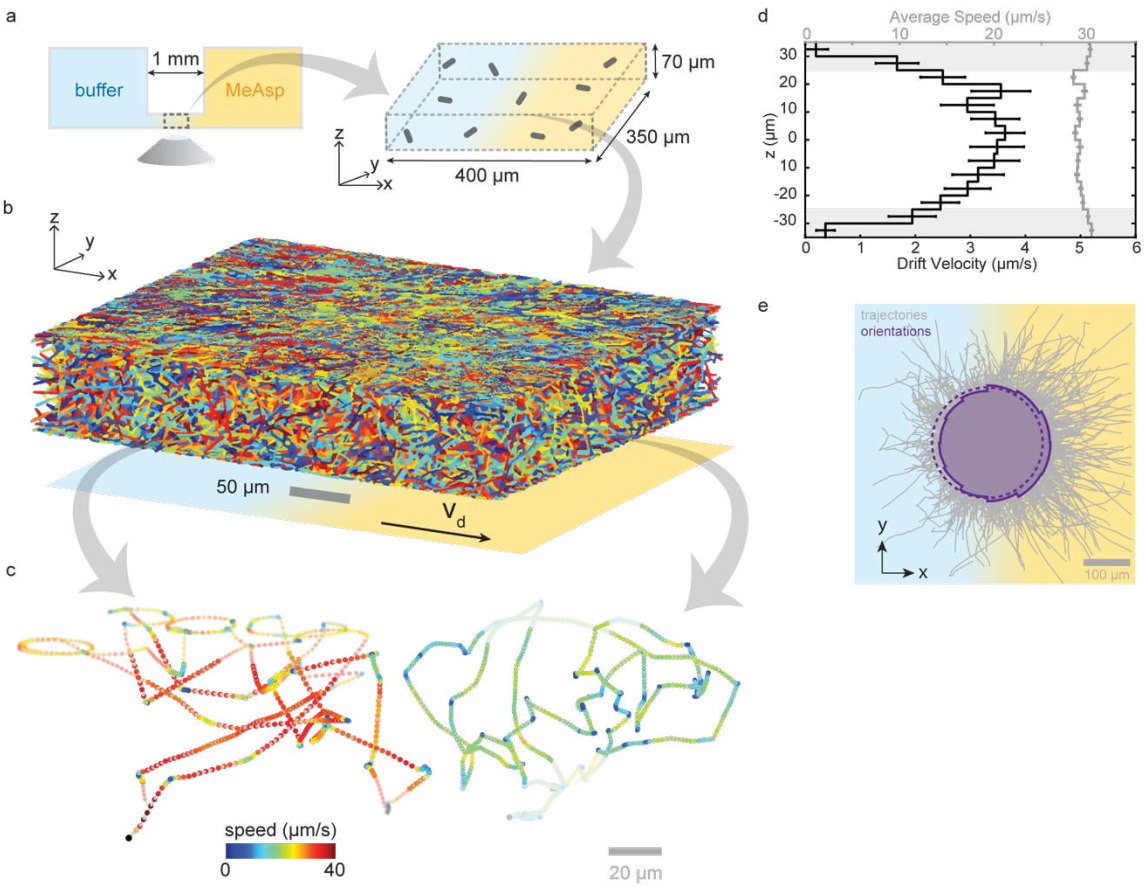

Fig. 1: Schematic of multiscale chemotaxis assay and its application to *E. coli* strain AW405. a) A quasi-static linear chemical gradient is established between two reservoirs containing a uniform concentration of bacteria. Bacteria are observed in the central portion of the linear gradient. b) 5,045 individual trajectories with a minimum duration of 5 frames and containing 37,080 s of total trajectory time, obtained in 9 min of recording at 15 Hz in a typical experiment. c) Two example trajectories (durations 63 s and 65 s) showing run-tumble motility in bulk solution and circular segments near the chamber surface (within 10 µm distance, faded). d) Drift velocity (black, defined as the average speed along the gradient direction, *x*) and average swimming speed (grey) as a function of height, *z*. Only bulk trajectories (defined as trajectory segments with a distance of more than 10 µm to the surface) are retained for further analysis. Error bars reflect standard errors of the mean. e) Bulk trajectories with aligned origins (grey) and polar probability distribution of instantaneous swimming directions projected in the *x*-*y* plane (purple, solid line). A flat distribution (dashed) is shown for reference.

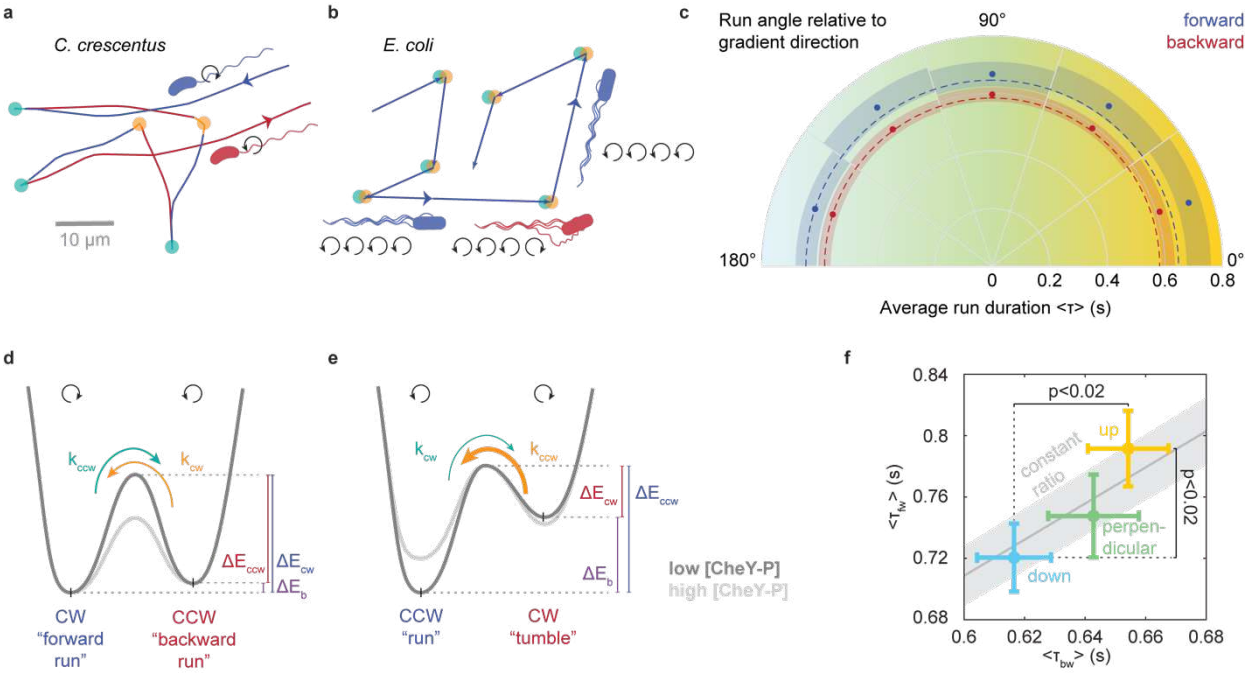

Fig. 2: *C. crescentus* chemotaxis. a) Example trajectory showing alternating backward (red) and forward (blue) runs, separated by switches in flagellar rotation direction that result in reversals (CW to CCW, teal) or flicks (CCW to CW, orange). b) Schematic of *E. coli* run-tumble motility. Runs are driven by CCW rotation (blue). Tumbles result from temporary CW rotation (red) of at least one flagellum and thus are bordered by two switches in rotation direction (CCW to CW, teal, CW to CCW, orange). c) Radial plot of average run durations (blue: forward, red: backward runs) as a function of projected angle to the *x*-axis in the *x*-*y* plane. The dashed lines indicate the average run durations observed for swimming down the gradient and serve to facilitate comparison. Shading indicates 95% confidence intervals. d) Schematic of 2-state motor rotation model proposed for *C. crescentus* and e) established for *E. coli*[26,27]. The energy difference ΔE_b (purple) between states determines the motor bias, while the energy barrier between states, ΔE_{ccw} and ΔE_{cw}, determines the switching rates, k_{cw} and k_{ccw}, respectively (see Supplementary Discussion). f) Average forward versus backward run durations, $\langle\tau_{fw}\rangle$ versus $\langle\tau_{bw}\rangle$, up (yellow), down (cyan) or perpendicular to (green) the gradient (defined by 36° cones around positive x-axis, negative x-axis, or y-axis, respectively). The solid line reflects a best-fit constant CW bias of 0.54 ± 0.01, with the standard error (Methods) shown as grey shading. P-values are shown for one-sided t-tests between durations up and down the gradient. Error bars reflect standard error of the mean.

Methods

Microfluidic device and gradient stability. Quasi-static chemical gradients are created in a commercially available microfluidic device (IBIDI µ-slide Chemotaxis) featuring an approximately 70 µm high, 1mm long, and 2 mm wide channel connecting two 65 µl reservoirs. Gradient establishment and stability over time were characterized for fluorescein gradients (10 µM/mm in MotM, see Supplementary Table 1 for media compositions) using a confocal microscope (Zeiss AXIO Imager.Z2). The 488 nm line was focused through a 20x water immersion objective and fluorescence emission collected in the 500–585 nm window with a pinhole adjusted to 30 µm diameter. A 4.5 h time series of line scans in the gradient direction across the center of the device was acquired after closing the device (Supplementary Fig. 1b). A large-scale 4x4 mm view of the device was obtained by tiling 2D scans (Supplementary Fig. 1a) acquired 5h after closing the device. The gradient is established within minutes of filling the device and shows a deviation of less than 4% from the final plateau value after 30 minutes (Supplementary Fig. 1c). No detectable variation in relative gradient magnitude is observed in the time range from 40 min to 4.5 h after filling the device (Supplementary Fig. 1c).

E. coli experiments

Bacterial culturing. Overnight cultures were inoculated from a frozen glycerol stock of *E. coli* AW405 (a kind gift of Howard Berg) in 2 ml TB and grown to saturation at 30°C, 250 rpm. Day cultures were inoculated with the overnight cultures at 1:200 dilution in 10 ml TB and grown at 33.5°C, 250 rpm, until they reached an optical density (OD) between 0.3 and 0.35 at 600nm. Volumes of 1 ml of bacterial culture were washed by three rounds of centrifugation in 1.5 ml microcentrifuge tubes (6 min at 2,000 rcf), each followed by gentle resuspension in 1 ml of motility medium MotM. They were diluted to a target OD of 0.003 (for acquisitions in a gradient) or 0.005 (no gradient) in MotM supplemented with 0.002% Tween 20, with or without chemoattractant, for injection into the chemotaxis device.

Sample preparation. The device's reservoirs were filled with the two bacterial solutions (with or without chemoattractant) following a modified version of the manufacturer's "Fast Method" protocol. First, the entire device was overfilled with buffer free of chemoattractant or bacteria through the filling ports, and then the central channel's ports were closed with plugs. 65 µl was removed from one reservoir, replaced by 65 µl of chemoattractant-free bacterial solution, and then this reservoir's ports were closed. Finally, all liquid was removed from the other reservoir and replaced with bacterial solution containing chemoattractant. Key to reproducible gradients is to not overfill this reservoir to avoid liquid flow in the central channel when the last two ports are closed. A uniform bacterial density across the device ensures that any population drift observed is not the result of a diffusive flux, but likely indicates chemotaxis. For control measurements, neither bacterial solution contained chemoattractant. At the bacterial densities used (OD of 0.005 or less), oxygen depletion is unlikely, and we do not observe a change in *E. coli* swimming speed in the reservoirs over the course of 1 h (Supplementary Fig. 1d).

Data acquisition. Phase contrast microscopy recordings were obtained at room temperature (~22°C) on a Nikon Ti-E inverted microscope using an sCMOS camera (PCO Edge 4.2) and a 40x objective lens (Nikon CFI SPlan Fluor ELWD 40x ADM Ph2, correction collar set to 1.2 mm to induce spherical aberrations[12]) focused at the center of the channel in all three dimensions. 3D bacterial trajectories were extracted[12] for a field of view of ~350 μm x 300 μm laterally (*x*, *y*) and over the entire depth (*z*) of the channel for typically several dozen individuals at a time. For *E. coli*, recordings were obtained starting from 50 minutes after filling the device. Three 3-min long recordings were obtained at 15 fps. Three replicates can be performed in parallel in half a day.

In-device conditions. We confirmed that the *E. coli* motile population we tracked in the central channel was representative of the whole population by also acquiring trajectories in one chamber during an experiment. The average speed of the motile population, defined as individuals having a mean swimming speed larger than 10 μm/s, in the reservoirs was stable in time and similar to that observed in the central channel (Supplementary Fig. 1d).

Data analysis. 3D Trajectories were extracted from phase contrast recordings using a high-throughput 3D tracking method based on image similarity between bacteria and a reference library[12]. Trajectories shorter than 5 frames were discarded. Positions were smoothed using 2nd order ADMM-based trend-filtering[28] with regularization parameter $\lambda = 1$, and speeds computed as forward differences in positions divided by the time interval between frames. All trajectories with an average speed below a threshold were considered non-motile and discarded. The threshold was set at 15 μm/s unless noted otherwise. The *z* position of the top and bottom of the chamber were identified by visual inspection of trajectory data. All trajectory segments within 10 μm of the top or bottom of the central channel were removed to avoid surface interaction effects, retaining 35% of total trajectory time. Fig. 1b shows data for one replicate. For Fig. 1d and e, we combine data from three biological repeats each yielding three recordings. The profile of the drift velocity as function of *z* position is similar in each replicate (Supplementary Fig. 1f). The drift velocity is the average of the *x* component of all 3D speed vectors from all bacteria. Across 3 biological replicates performed in parallel, we obtain a drift velocity of 2.7 ± 0.3 μm/s (mean ± SD across the replicates) for *E. coli* in a 10 μM/mm MeAsp gradient, and observe no chemotactic drift along either the *y* or *z* axis (0.1 ± 0.3 μm/s and 0.09 ± 0.1 μm/s, respectively). Biological replicates performed on other days yielded drift velocities of 2.7 μm/s and 2.5 μm/s. A control chamber without a gradient showed no drift either (0.34 ± 0.8 μm/s along *x*). For data obtained from a single experiment (Supplementary Fig. 1e), we estimate the noise on the drift measurement by a jackknife resampling procedure consisting of dividing the data into subsets of 150 trajectories and computing the standard error of the mean drift obtained for different subsets. For drift as a function of *z,* trajectories are first sliced into segments by *z* bin, and jackknifing is performed for each *z* bin.

C. crescentus **experiments**

Bacterial culturing and sample preparation. Overnight cultures were inoculated from individual *C. crescentus* (CB15, ATCC 19089) colonies, grown on 1.5% agar PYE plates streaked from glycerol stock, and grown to saturation in 2 ml PYE at 30°C, 200 rpm. Day cultures were inoculated at a dilution of 1:20 (v/v) in M2G[29] or PYE and grown to an OD600 of at least 0.3 (a few hours for PYE,

around 12 hours for M2G). Because the cell-cycle dependent motility of *C. crescentus* is quickly lost, we opted to grow the cells directly inside the device and let them produce swarmer cells while the gradient is being established. To this end, the day culture was again diluted 1:1 in fresh medium and injected into both reservoirs of the device which was then incubated at room temperature. When the chamber walls were colonized by a sufficient density of stalked cells as determined by visual inspection under the microscope (a few hours for PYE, 2 days for M2G), the device was rinsed several times with fresh M2G, until no swimming bacteria were observed. Then fresh M2G and 1 mM xylose/M2G, respectively, were injected into the reservoirs to create a 1 mM/mm xylose gradient in the central channel. Xylose is a known chemoattractant for *C. crescentus*[21,30].

Data acquisition. Because of the cell cycle-dependent chemotaxis[16] of *C. crescentus*, we favored acquiring data as early as possible over waiting for perfect gradient stability. Recordings spanning 2.5 minutes at 30 fps were acquired from 20 to 55 minutes after closing the device, in five biologically independent experiments, totaling a cumulated acquisition time of 75 minutes.

Data analysis. Trajectories were obtained and smoothed as for *E. coli*, except for the ADMM regularization parameter being set to $\lambda = 0.3$. To account for the layer of attached cells lining the surface, only segments with a distance of more than 13 μm from the top or bottom chamber surface were retained to avoid surface interaction effects. Supplementary Table 2 details statistical characteristics of the subsets of data used for analysis. Standard errors on drift velocities are obtained by jackknifing as described for *E. coli*.

Run-reverse-flick analysis. The turning event detection is based on the local rate of angular change, computed from the dot product between the sums of the two consecutive velocity vectors preceding and subsequent to a time point. The threshold for a turn to begin is an α-fold rate relative to the median rate of angular change rate of the run segments, as determined in three iterations of the procedure. We determined by visual inspection of trajectories that a factor $\alpha = 6$ gave satisfactory results. A new run begins with at least two time points (at least 0.066 s) under this threshold. Backward (CCW rotation) and forward (CW rotation) runs were identified as runs with a turn under 130°, respectively at the end or at the beginning the run, and a turn above 150° at the other end of the run. A total of 5,342 backward and 2,898 forward runs were identified within a subpopulation of 6,230 trajectories.

Run duration analysis. Runs are considered to be going up or down the gradient if they fall within a 36° cone around the positive, respectively negative, *x* axis. The value of 36° was chosen so as to balance a trade-off between maximizing the number of contributing runs with maximizing their alignment with the gradient direction. The conclusions are not sensitive to the exact value chosen. The fact that runs going up the gradient are longer than those going down the gradient confirms that the observed drift, though small, is indeed caused by chemotaxis. We determine maximum-likelihood inverse Gaussian distributions from the run duration data:

$$f = \sqrt{\frac{\lambda}{2\pi\tau^3}} \exp\left(-\frac{\lambda(\tau-\mu)^2}{2\mu^2\tau}\right)$$

where the run duration τ, the mean, μ, and the shape parameters, λ, are strictly positive. We obtain the following parameters: $\mu = 0.79$ s, $\lambda = 1.18$ s, and $\mu = 0.72$ s, $\lambda = 1.21$ s, for forward runs going up and down the gradient, respectively; and $\mu = 0.65$ s, $\lambda = 1.85$ s, and $\mu = 0.62$ s, $\lambda = 1.78$ s, for backward runs going up or down the gradient, respectively.

Motor bias analysis. To determine a best-fit motor bias for Fig. 2c, an orthonormal linear fit constrained to a zero intercept is applied to the average run durations up, down, and perpendicular to the gradient. The error on the slope is estimated as the standard deviation of slopes obtained by fitting data generated in a Monte Carlo procedure, consisting of drawing data points randomly from Gaussian distributions centered about the actual data points and with a standard deviation matching the data points' standard error. The CW bias, b_{CW}, can be obtained from the slope, s, as $b_{CW} = s/(1+s)$. We obtain $s = 1.18 \pm 0.03$, corresponding to $b_{CW} = 0.54 \pm 0.01$.
Run speed analysis. To determine the ratio of forward to backward swimming speed for Supplementary Fig. 2e, average speeds were computed across all forward and backward runs, respectively, for each trajectory in subset 8 (see Supplementary Table 2). An orthonormal linear fit constrained to zero intercept yields a slope of 1.025 ± 0.002 (SE).

References

1 Matilla, M. A. & Krell, T. The effect of bacterial chemotaxis on host infection and pathogenicity. *FEMS Microbiology Reviews* **42**, 202, doi:10.1093/femsre/fux052 (2018).

2 Raina, J.-B., Fernandez, V., Lambert, B., Stocker, R. & Seymour, J. R. The role of microbial motility and chemotaxis in symbiosis. *Nature Reviews Microbiology* **292**, 1096, doi:10.1038/s41579-019-0182-9 (2019).

3 Seymour, J. R., Amin, S. A., Raina, J.-B. & Stocker, R. Zooming in on the phycosphere: the ecological interface for phytoplankton-bacteria relationships. *Nature microbiology* **2**, 17065, doi:10.1038/nmicrobiol.2017.65 (2017).

4 Adler, J. A Method for Measuring Chemotaxis and Use of the Method to Determine Optimum Conditions for Chemotaxis by Escherichia coli. *Journal of general microbiology* **74**, 77-91, doi:10.1099/00221287-74-1-77 (1973).

5 Colin, R., Zhang, R. & Wilson, L. G. Fast, high-throughput measurement of collective behaviour in a bacterial population. *Journal of The Royal Society Interface* **11**, 20140486-20140486, doi:10.1098/rsif.2014.0486 (2014).

6 Berg, H. C. & Brown, D. A. Chemotaxis in Escherichia coli analysed by Three-dimensional Tracking. *Nature* **239**, 500-504, doi:10.1038/239500a0 (1972).

7 Larsen, S. H., Reader, R. W., Kort, E. N., Tso, W.-w. & Adler, J. Change in direction of flagellar rotation is the basis of the chemotactic response in Escherichia coli. *Nature* **249**, 74-77, doi:10.1038/249074a0 (1974).

8 Webre, D. J., Wolanin, P. M. & Stock, J. B. Bacterial chemotaxis. *Current Biology* **13**, R47-49 (2003).

9 Xie, L., Altindal, T., Chattopadhyay, S. & Wu, X.-l. Bacterial flagellum as a propeller and as a rudder for efficient chemotaxis. *Proceedings of the National Academy of Sciences* **108**, 2246-2251, doi:10.1073/pnas.1011953108 (2011).

10 Cai, Q., Li, Z., Ouyang, Q., Luo, C. & Gordon, V. D. Singly Flagellated Pseudomonas aeruginosa Chemotaxes Efficiently by Unbiased Motor Regulation. *mBio* **7**, e00013, doi:10.1128/mBio.00013-16 (2016).

11 Spudich, J. L. & Koshland, D. E. Non-genetic individuality: chance in the single cell. *Nature* **262**, 467-471 (1976).

12 Taute, K. M., Gude, S., Tans, S. J. & Shimizu, T. S. High-throughput 3D tracking of bacteria on a standard phase contrast microscope. *Nature Communications* **6**, 1-9, doi:10.1038/ncomms9776 (2015).

13 Lauga, E., DiLuzio, W. R., Whitesides, G. M. & Stone, H. a. Swimming in Circles: Motion of Bacteria near Solid Boundaries. *Biophysical Journal* **90**, 400-412, doi:10.1529/biophysj.105.069401 (2006).

14 Waite, A. J. *et al.* Non‐genetic diversity modulates population performance. *Molecular Systems Biology* **12**, 895-814, doi:10.15252/msb.20167044 (2016).

15 Morse, M., Colin, R., Wilson, L. G. & Tang, J. X. The Aerotactic Response of Caulobacter crescentus. *Biophysical Journal* **110**, 2076-2084, doi:10.1016/j.bpj.2016.03.028 (2016).

16 Laub, M. T., McAdams, H. H., Feldblyum, T., Fraser, C. M. & Shapiro, L. Global Analysis of the Genetic Network Controlling a Bacterial Cell Cycle. *Science* **290**, 2144-2148, doi:10.1126/science.290.5499.2144 (2000).
17 Alley, M. R., Maddock & Shapiro, L. Requirement of the carboxyl terminus of a bacterial chemoreceptor for its targeted proteolysis. *Science* **259**, 1754-1757, doi:10.1126/science.8456303 (1993).
18 Liu, B. *et al.* Helical motion of the cell body enhances Caulobacter crescentus motility. *Proceedings of the National Academy of Sciences* **111**, 11252-11256, doi:10.1073/pnas.1407636111 (2014).
19 Nesper, J. *et al.* Cyclic di-GMP differentially tunes a bacterial flagellar motor through a novel class of CheY-like regulators. *eLife* **6**, 550, doi:10.7554/eLife.28842 (2017).
20 Morse, M., Bell, J., Li, G. & Tang, J. X. Flagellar Motor Switching in Caulobacter CrescentusObeys First Passage Time Statistics. *Physical Review Letters* **115**, 312, doi:10.1103/PhysRevLett.115.198103 (2015).
21 Ely, B. *et al.* General nonchemotactic mutants of Caulobacter crescentus. *Genetics* **114**, 717-730 (1986).
22 Koyasu, S. & Shirakihara, Y. Caulobacter crescentus flagellar filament has a right-handed helical form. *Journal of Molecular Biology* **173**, 125-130 (1984).
23 Berke, A. P., Turner, L., Berg, H. C. & Lauga, E. Hydrodynamic Attraction of Swimming Microorganisms by Surfaces. *Physical Review Letters* **101**, 038102-038104, doi:10.1103/PhysRevLett.101.038102 (2008).
24 Magariyama, Y. *et al.* Difference in Bacterial Motion between Forward and Backward Swimming Caused by the Wall Effect. *Biophysical Journal* **88**, 3648-3658, doi:10.1529/biophysj.104.054049 (2005).
25 Mao, H., Cremer, P. S. & Manson, M. D. A sensitive, versatile microfluidic assay for bacterial chemotaxis. *Proceedings of the National Academy of Sciences* **100**, 5449-5454, doi:10.1073/pnas.0931258100 (2003).
26 Khan, S. & Macnab, R. M. The steady-state counterclockwise/clockwise ratio of bacterial flagellar motors is regulated by protonmotive force. *Journal of Molecular Biology* **138**, 563-597, doi:10.1016/S0022-2836(80)80018-0 (1980).
27 Scharf, B. E., Fahrner, K. A., Turner, L. & Berg, H. C. Control of direction of flagellar rotation in bacterial chemotaxis. *Proceedings of the National Academy of Sciences* **95**, 201-206 (1998).
28 Boyd, S., Parikh, N., Chu, E., Peleato, B. & Eckstein, J. Distributed Optimization and Statistical Learning via the Alternating Direction Method of Multipliers. *Foundations and Trends in Machine Learning* **3**, 1-122, doi:10.1561/2200000016 (2011).
29 Ely, B. Genetics of Caulobacter crescentus. *Methods in Enzymology* **204**, 372-384, doi:10.1016/0076-6879(91)04019-K (1991).
30 Kovarik, M. L. *et al.* Microchannel-nanopore device for bacterial chemotaxis assays. *Analytical Chemistry* **82**, 9357-9364, doi:10.1021/ac101977f (2010).

Author contributions

K.M.T. conceived the research, M.G. and K.M.T. designed the experiments, M.G. performed all experiments and analysis, M.G. and K.M.T. interpreted the data and wrote the manuscript.

Acknowledgements

We thank H. Berg for providing *E. coli* strain AW405, and H. Berg, B.G. Hosu, S. Crosson, A. Fiebig, D. Hershey, N. Cira, A.W. Murray, and M. Burns for helpful comments on the manuscript. This research was funded by the Rowland Institute at Harvard.

Data availability

All data and computer code are available from the authors upon reasonable request.

Conflict of Interests

The authors declare that they have no conflict of interest.

Figures

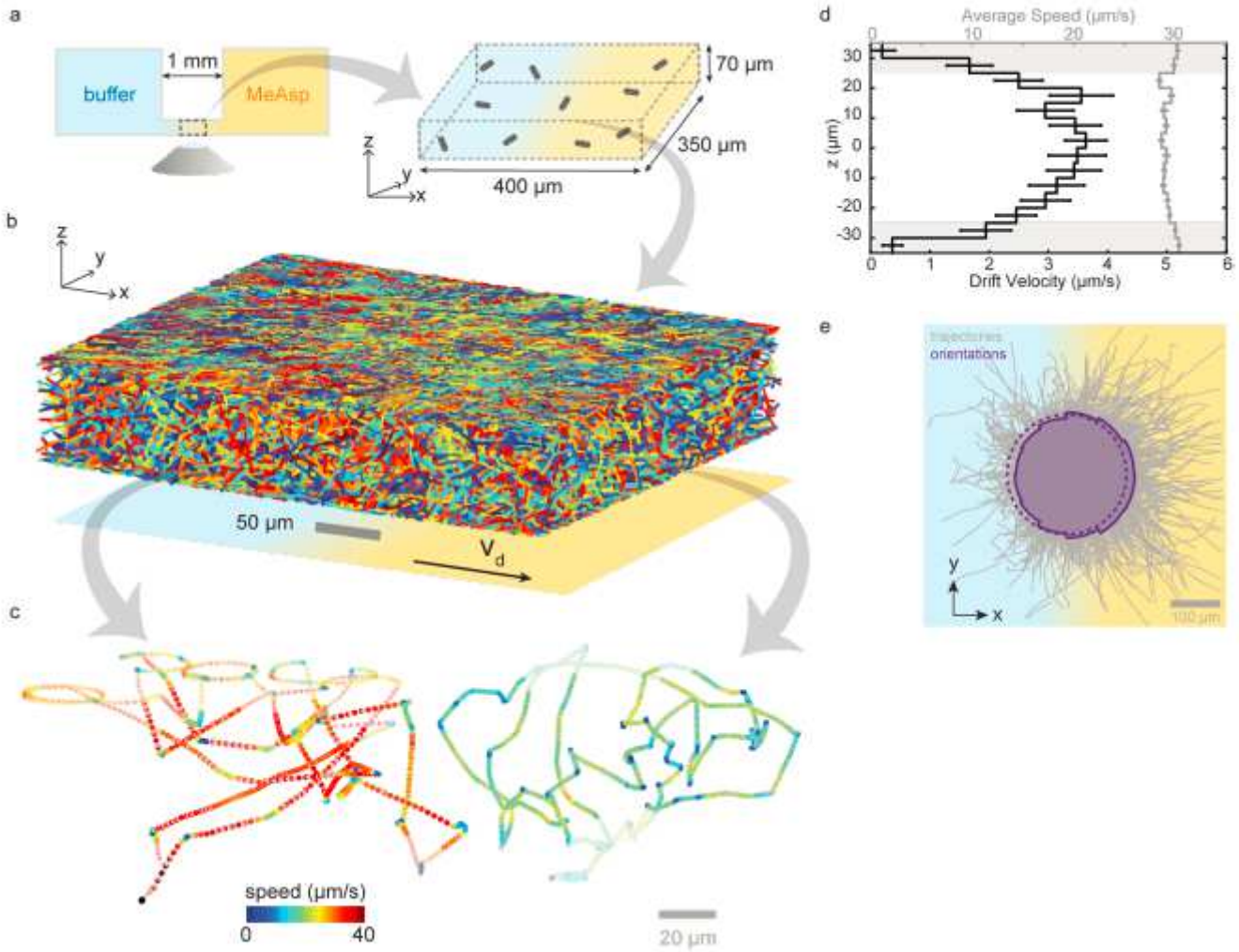

Figure 1

Schematic of multiscale chemotaxis assay and its application to E. coli 1 strain AW405. a) A quasi-static linear chemical gradient is established between two reservoirs containing a uniform concentration of bacteria. Bacteria are observed in the central portion of the linear gradient. b) 5,045 individual trajectories with a minimum duration of 5 frames and containing 37,080 s of total trajectory time, obtained in 9 min of recording at 15 Hz in a typical experiment. c) Two example trajectories (durations 63 s and 65 s) showing run-tumble motility in bulk solution and circular segments near the chamber surface (within 10 µm distance, faded). d) Drift velocity (black, defined as the average speed along the gradient direction, x) and average swimming speed (grey) as a function of height, z. Only bulk trajectories (defined as trajectory segments with a distance of more than 10 µm to the surface) are retained for further analysis. Error bars reflect standard errors of the mean. e) Bulk trajectories with aligned origins (grey) and polar probability distribution of instantaneous swimming directions projected in the x-y plane (purple, solid line). A flat distribution (dashed) is shown for reference.

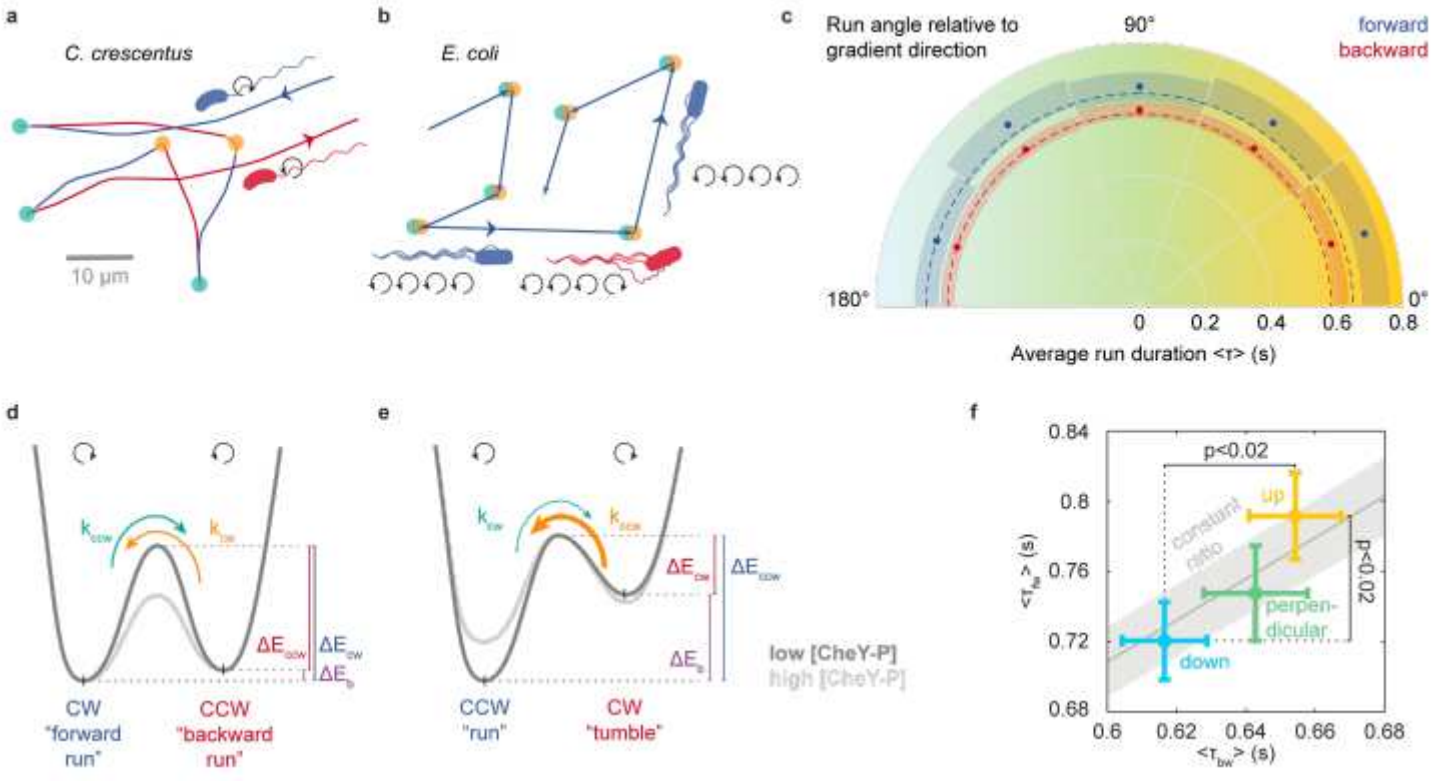

Figure 2

C. crescentus chemotaxis. a) Example trajectory showing alternating backward (red) and forward (blue) runs, separated by switches in flagellar rotation direction that result in reversals (CW to CCW, teal) or flicks (CCW to CW, orange). b) Schematic of E. coli run-tumble motility. Runs are driven by CCW rotation (blue). Tumbles result from temporary CW rotation (red) of at least one flagellum and thus are bordered by two switches in rotation direction (CCW to CW, teal, CW to CCW, orange). c) Radial plot of average run durations (blue: forward, red: backward runs) as a function of projected angle to the x-axis in the x-y plane. The dashed lines indicate the average run durations observed for swimming down the gradient and serve to facilitate comparison. Shading indicates 95% confidence intervals. d) Schematic of 2-state motor rotation model proposed for C. crescentus and e) established for E. coli26,27. The energy difference ΔEb (purple) between states determines the motor bias, while the energy barrier between states, ΔEccw and ΔEcw, determines the switching rates, kcw and kccw, respectively (see Supplementary Discussion). f) Average forward versus backward run durations, <τfw> versus <τbw>, up (yellow), down (cyan) or perpendicular to (green) the gradient (defined by 36° cones around positive x-axis, negative x-axis, or y-axis, respectively). The solid line reflects a best-fit constant CW bias of 0.54 ± 0.01, with the standard error (Methods) shown as grey shading. P-values are shown for one-sided t-tests between durations up and down the gradient. Error bars reflect standard error of the mean.

Supplementary Files

This is a list of supplementary files associated with this preprint. Click to download.

- SupplementaryInformation.pdf